1 November 2019
djunes.janssens@vub.be

CERN summer student program rapport: A better understanding of gas gain simulations in GEM detectors

Djunes Janssens
Supervisors: Rob Veenhof, Eraldo Oliveri & Heinrich Schindler
EP-DT-DD, CERN.

Keywords: GEM, gas gain, Garfield++, ANSYS, hole geometry, CERN summer student project

Contents

1 Introduction

Invented by Fabio Sauli in 1997, the Gaseous Electron Multiplier (GEM) falls under the category of micro-pattern gaseous detectors (MPGDs) and consists of a perforated, very thin, two-side metal-clad polymer foil [1]. The main material used in its production process is a 50 μm thick polyimide foil with two layers of metal (mainly copper) on opposite sides. The holes in the polyimide and the metals, around 100 per square millimeter, are created by employing a chemical etching technique and have a diameter of about 70 μm. A schematic representation of a triple GEM detector can be found in figure 1. This setup is placed in a closed environment filled with a particular gas mixture, e.g. Ar-CO_2. This allows for position detection of ionizing radiation coming from charged particles, photons, X-rays, and neutrons tracking through the gas by the collection of primary electrons, i.e. electrons generated due to ionization caused by the incident radiation. The collection of the primary electrons on a readout plane without any multiplication stage would give a poor signal-to-noise ratio. The addition of the GEM foils improves this. Upon applying a voltage (V_{GEM}) across the GEM electrodes, a strong dipole field develops in and around the holes. Due to the Lorentz force, the primary electrons can gain enough energy to ionise the gas themselves, thereby introducing new free electrons. This process can be repeated, resulting in the characteristic Towsend avalanches, which are depicted in figure 1. These are primarily formed at the bottom of the holes, close to the copper edges, a place that can be reached by diffusion. The increase in charge that is collected by the readout plane significantly increases the signal-to-noise ratio of the measured signal [3]. Due to the high rate tracking capability of the GEM detector, it is widely used in high-energy physics experiments such as in muon systems of CMS and LHCb as well as in the ALICE TPC [4, 5, 6]. Over the last few years a considerable amount of work has been done to improve the simulations of MPGDs. Unfortunately, a full

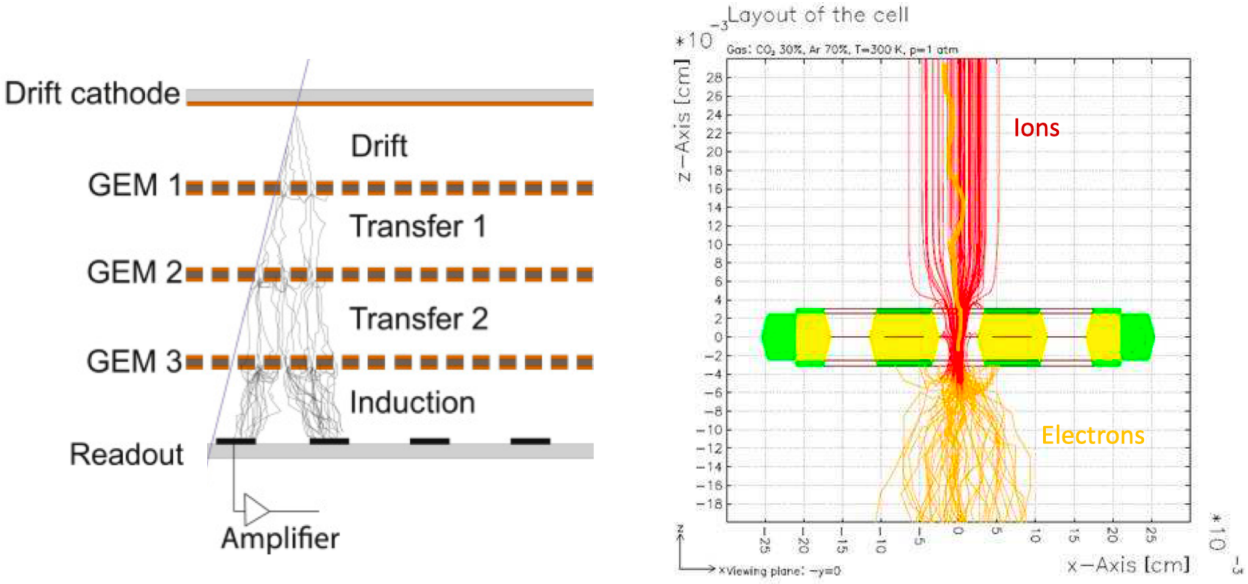

Figure 1: **Right:** Simplified depiction of a triple GEM detector setup and Towsend avalanches. **Left:** Cross-sectional view of the trajectories of the electrons (yellow) and ions (red) in assimilated Towsend avalanches for a single GEM foil [2].

understanding of the physics behind MPGDs is still missing, but is vital for the improvement of such detectors.

The terminology used in this document is the following. Total or absolute gas gain: the multiplication factor between the original and final amount of charges. Because of electron attachment in which a free electron is kept by a neutral molecule; and recombination in which an electron is absorbed by a positive ion, not all free electrons will reach the anode. In addition, some of the charges will end up on the surface of the copper or polyimide, as can be seen in figure 1. This accumulation of charge over time can significantly alter the absolute gas gain. This is called the charge up effect [7]. The loss of charge leads to the notion of the effective or measured gas gain: the net charges reaching the anode plane in a GEM, per incident primary charge, exclusive of losses. Gas gain, in general, can refer to both cases. The efficiency will refer to the ratio between the effective and absolute gas gain.

Figure 2 compares measured gas gains as a function of the voltage across the GEM with the calculated effective gas gain using theory. A discrepancy of a factor 2.2468 ± 0.2640 can be observed over a V_{GEM} range of $300 - 500$ V and will be referred to as the discrepancy factor. This inconsistency between experiment and theory has been around for more than 10 years and has been independently observed [2]. The aim of this project was to improve the

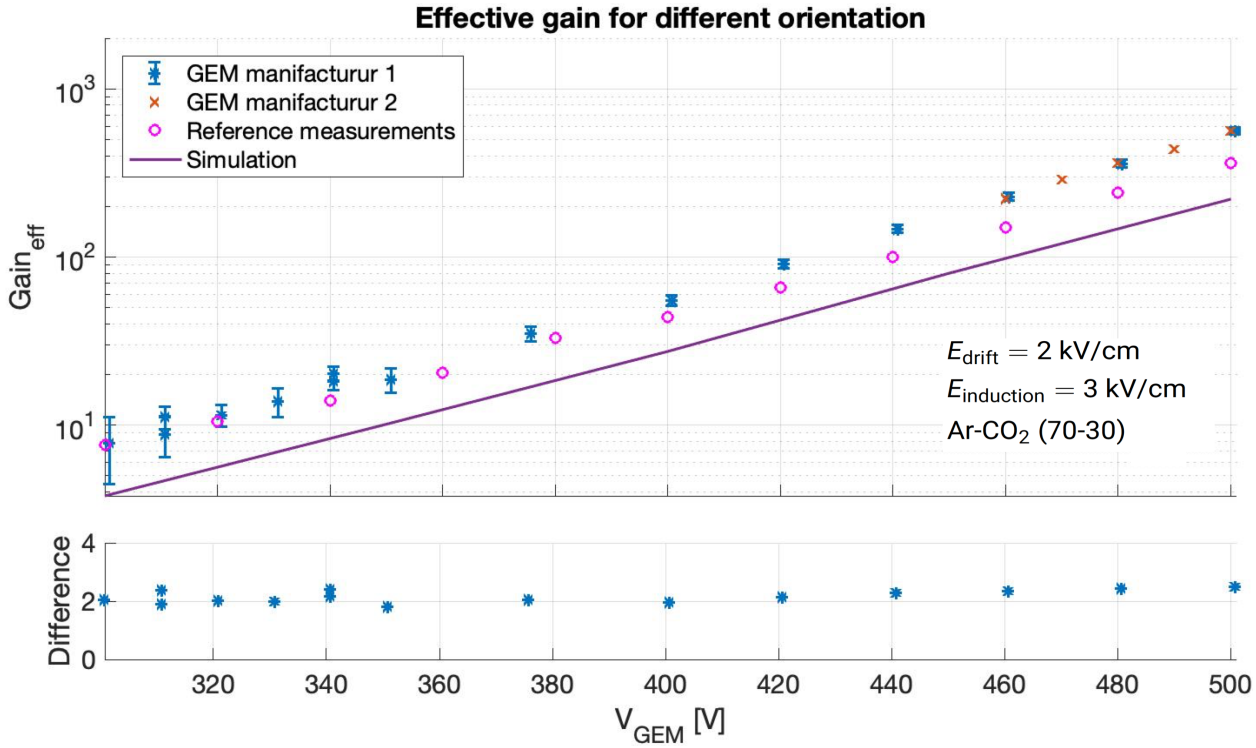

Figure 2: Comparison between measured and calculated effective gas gain as a function of V_{GEM} of a single GEM detector. Measurements are performed with GEM foils of different batches to indicate the consistency of the problem. A discrepancy factor $2,2468 \pm 0,2640$ between simulations and batch 1 GEMs can be observed. These measurements and calculations are described in sections 2 and 3, respectively. Similar results can be found in reference [2], which are plotted in pink.

understanding of the observed difference between experimentally obtained and theoretically calculated effective gas gains in GEM detectors. This document provides a short overview of the topics handled during the project and the results. Unfortunately, we were not able to resolve the discrepancy. However, more insight into different aspects of the GEM were obtained in the process.

During the project, different avenues of exploration were considered. These will be presented in this document in two major parts. The first part, section 2, will focus on the results of measurements of the effective gas gain and the charge up effect of a single GEM detector will be presented. In addition, scanning electron microscope (SEG) measurements of the geometry of the GEM holes will be discussed, shedding more light on the GEM foil orientation dependency of the gas gain. In the second part of this document, section 3, the methodology used to calculate the absolute and effective gas gain will be given. With this the surface potential of the polyimide will be compared to analytically obtained solutions. An modification to the electron transport algorithm of Garfield++ [8] by using Runge-Kutta-Nyström method will be described and its effects on the gas gain. Additionally, gas gain dependency secondary electron emissions and geometry of the GEM hole.

2 Measurements

2.1 Setup

A schematic representation of the experimental setup is given by figure 3. A triple GEM detector was configured to function as a single GEM detector by using the second GEM foil as an anode. This greatly simplifies the simulation model used for comparison with the measurements. The assembly of the detector was done is such a way that the top foil would have the lowest leakage current of the three, namely 3.0 ± 0.5 nA. The foils are produced as a CERN standard single GEM; the parameters of this template are given in table 1. The SEG measurements of the geometry of a hole in the top GEM can be found in subsection 2.4. This triple setup was placed in an enclosed volume where a gas mixture of Ar-CO_2 70-30%

Table 1: Specifications of a CERN standard GEM [9].

Parameter	Value
Area	10x10 cm^2
Metal thickness	5 μm
Polyimide thickness	50 μm
Outer diameter	70 μm
Inner diameter	50 μm
Pitch	140 μm
Drift gap	3 μm
Induction gap	2 μm

has a continuous gas flow. All measurements are performed at 1 atm pressure and with a surrounding temperature of 22 ^{o}C. These are considered exact. As X-ray source, different Fe_{55} sources with varying rates were used to expand the range of voltages across the GEM

that could be measured, i.e. low rate sources for high voltages to avoid sparking and high rate sources for low voltages to have a measurable signal.

The cathode, top, and bottom of the GEM foil were connected to three separate channels of the CAEN® NDT1471H high voltage power supply [10]. This enables us to vary the field intensities in the different regions of the detectors (i.e. the drift field, the field across the GEM, and the induction field) independently from one another. When electron avalanches are created inside the GEM holes, they give rise to a voltage signal that can be observed by connecting an amplifier. In this case, the ORTEK® model 450 was set up between the bottom of the GEM foil and an oscilloscope [11]. A pulse height spectrum is then obtained by using an AMPTEK® MCA-8000D (MCA), which measures these pulses [12]. A clean signal has a prominent photo-peak, a clear escape peak and a noise pedestal, each of which is well separated from one another. The measured spectrum is subject to uncertainties coming from the apparatus, less than 0.8%, and pile-up, which refers to the overlap of consecutive signals which are not treated as different [12]. To overestimate this effect, an uncertainty of 5% is introduced. Additional uncertainties on parameters derived from the spectrum, e.g. main peak position, can occur due to fitting. To determine the number of electrons that reach the anode, a current readout was performed by a Keithley® model 6487 every 1.0860 s on an amplified signal coming out of the ORTEC 142PC preamplifier [11, 13]. The uncertainty on the current measurement was determined by the standard deviation when taking the average of ten consecutive measurements.

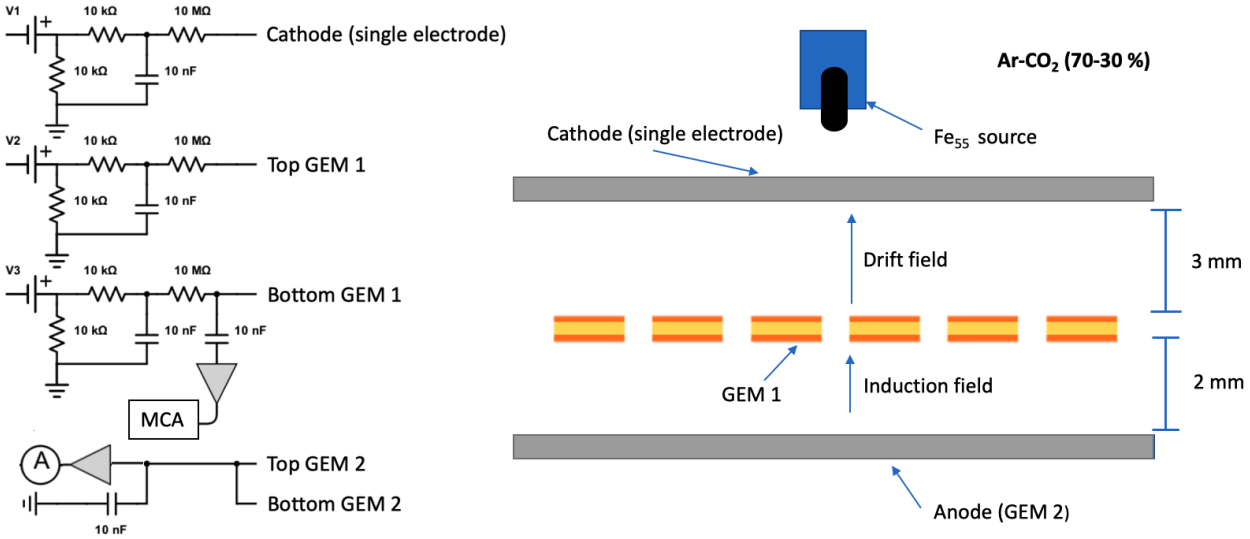

Figure 3: A schematic representation of the triple GEM experimental setup functioning as a single GEM setup through the use of the second GEM foil as the anode.

2.2 Effective gas gain

The effective gas gain G_{eff} can be determined using the measured current difference on the anode I between signal with and without the X-ray source; this is shown in figure 4. The

relation is given by

$$G_{\text{eff}} = \frac{I}{en_0 f^*}\,, \tag{1}$$

where e is the charge of the electron, n_0 the amount of primary electrons created per incident photon and f^* the effective rate of the Fe_{55} source [3]. The latter needs to determined using the MCA spectrum, which is shown in figure 4. Here the area of the spectrum, i.e. the total

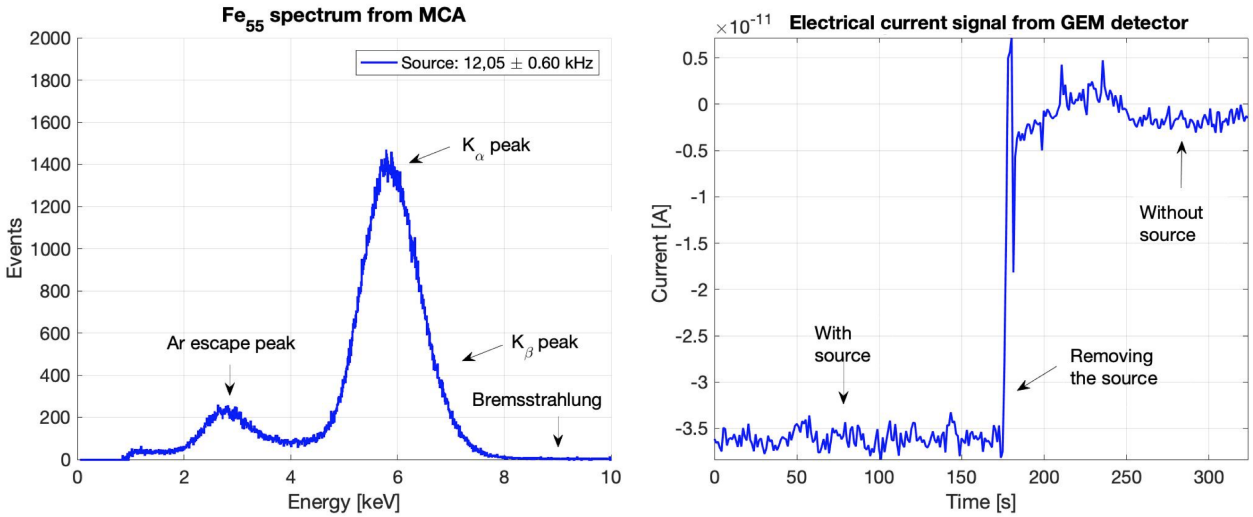

Figure 4: These measurements were performed with $E_{\text{drift}} = 2$ kV/cm, $E_{\text{ind}} = 3$ kV/cm and $V_{\text{GEM}} = 420$ V. **Left:** MCA spectrum of a Fe_{55} source with background subtraction obtained by voltage difference on the bottom plate of the GEM foil due the avalanches in the holes. Hear the characteristic structures of the spectrum are indicated. **Right:** Current readout from the anode when removing the X-ray source.

count of events, divided by the sampling time of 30 s gives f^* after background subtraction. The number of primary electrons created per incident photon is estimated by analyzing the MCA spectrum. This is done by fitting the peaks of individual channels on a are calibrated energy axis. The number of electrons contributed by individual channel is obtained from

$$n_0 = \sum_i \left(\frac{n_i E_i}{W \sum_j n_j} \right)\,, \tag{2}$$

where n_i is the number of counts and E_i is the energy corresponding to the i'th channel of the MCA. W is the work function of Ar-CO_2 70-30% mixture as obtained from reference [14]. The number of electrons per incident electron is $n_0 = 196.6 \pm 1.8$ [15]. The measurements were performed after letting the GEM fully charge up for ~ 2 hours, as further explained in subsection 2.5. Using equation (1), the effective gain of the detector was measured as a function of V_{GEM}. Figure 5 presents the results for $E_{\text{drift}} = 2$ kV/cm, $E_{\text{ind}} = 3$ kV/cm which is the same field configuration as [2]. This data was fit by a function of the form

$$G_{\text{eff}} = \exp(aV_{\text{GEM}} + b)\,, \tag{3}$$

with a and b the fitting parameters. The resulting fit gives a and b values of 0.02162 ± 0.00025 V^{-1} and -4.503 ± 0.1055 (no units) respectively.

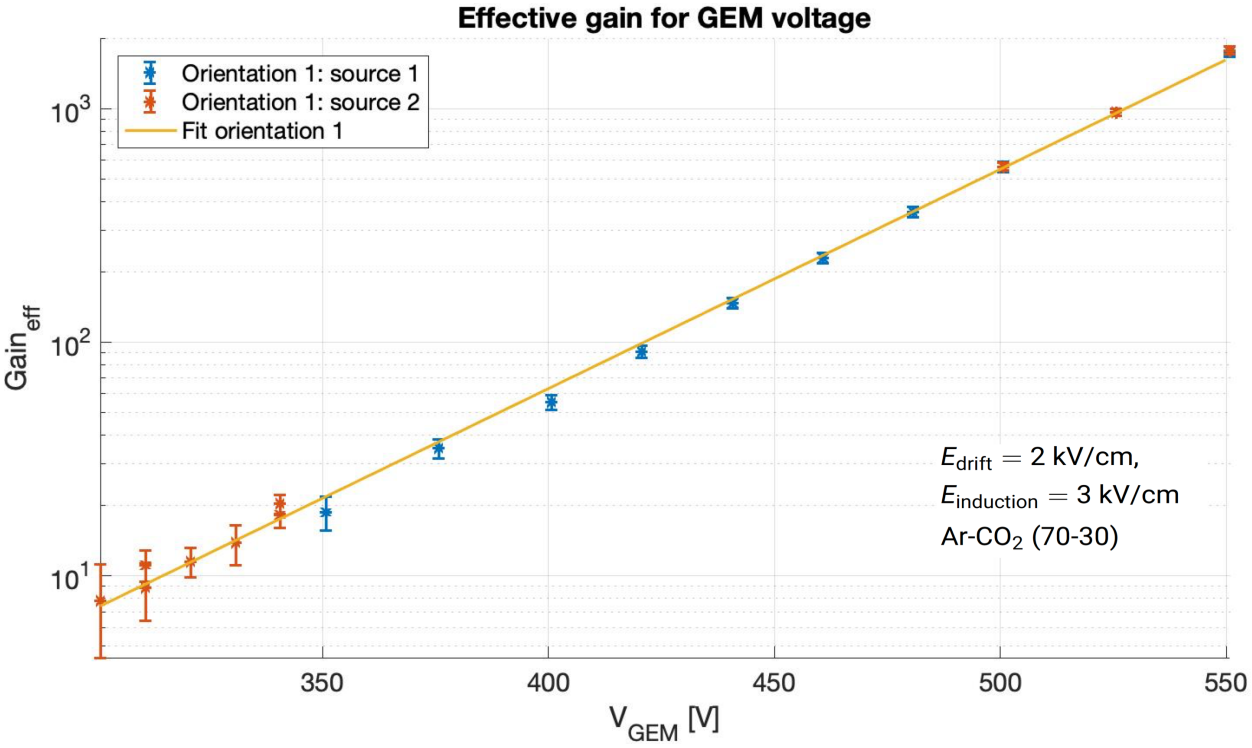

Figure 5: Measured effective gain for two different sources: 12.045 ± 0.602 kHz and 16.974 ± 0.8487 kHz for sources 1 and 2, respectively. The data points were fit by the form (3) with Chi-square value $\chi^2 = 1.1575$. The label "orientation 1" is there to distinguish it with the case where the GEM is flipped, as seen later.

The effective gain is related to the collection and extraction efficiency of the detector. The primary charge collection depends on the intensity of the drift field; when the drift field strength is too low, charges will be partially lost due to recombination. In contrast, if this field is too high, part of the primary electrons will be lost due to the field lines guiding them to the top surface of the GEM foil. Between these extreme cases, there is a plateau region, where almost all primary charge will be collected in the GEM holes. The induction field defines the fraction of the avalanche electrons that go to the anode instead of the bottom GEM electrode. This extraction efficiency will increase if the value of this field augments. The influence of the external fields (drift and induction fields) on measured effective gas gain is determined by varying one while keeping the other at a fixed value [2]. This dependency can be quantified by the position of the main peak position in the MCA spectrum, i.e. the K_α peak centroid on a non-calibrated scale, which is proportional to the gas gain of the detector. This center of the peak was determined by doing local Gaussian fits of the Fe_{55} spectra at different field strengths. Figure 6 shows that the drift field strengths used in figure 6 are in the plateau, indicating that all the maximum ionization current is collected. In addition, it shows a strong induction field dependence, giving an incentive to take this into account when comparing results.

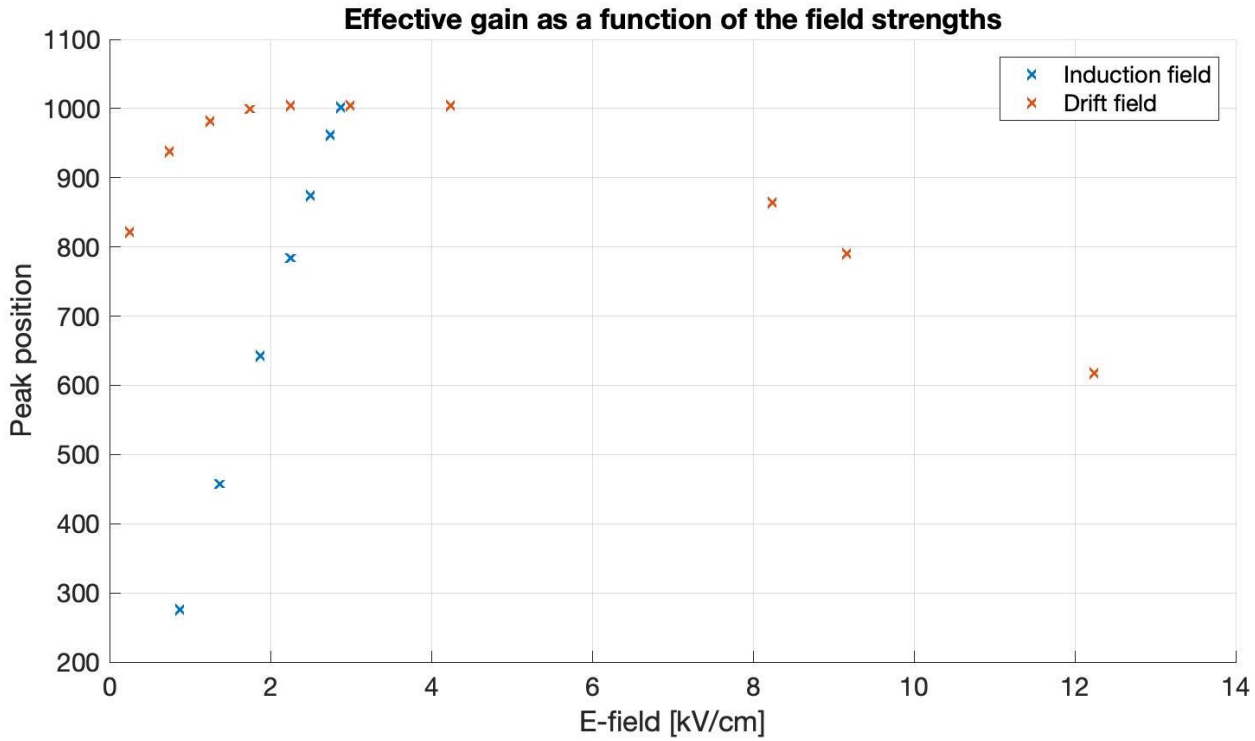

Figure 6: The measurements performed have a drift field strength, $E_{\text{drift}} = 2$ kV/cm, which is in the plateau region. Small variations from this value lead to a minor difference to the measured effective gas gain as long as it is in this saturation value. On the contrary, two slightly different induction field intensities give significantly different effective gas gains. The uncertainties are not plotted due to them being too small for visualization.

2.3 Orientation of the GEM

Table 1 shows the characteristic parameters of a CERN standard GEM. In the manufacturing of the GEM foils, two main production techniques are used: double-mask and single-mask. A schematic comparison in given by figure 7. In the double-mask technique, a standard GEM foil is manufactured with photoresist lamination on the upper and lower copper layers. This allows for chemical etching on both sides, creating a hole when the chemicals reach the middle of the foil. The uniformity of the alignment across the foil becomes progressively more difficult to achieve since they are primarily performed by hand. An alternative way to overcome this difficulty is the single-mask process. By using only one mask to the pattern only the top copper layer, no alignment needs to be done. The bottom copper layer is etched after the polyimide, using the holes in the polyimide as a mask [3, 16].

Both methods can result in deformations of the perfect double cone geometry, which are primarily used in simulations. This could lead to different gains of the detector. These deviations can lead to an asymmetrical geometry of the GEM hole with respect to the center of the foil; this is especially true for single-mask foils. As a result, a dependency of the gas gain on the orientation of the GEM foil can be seen. This has been observed for a triple GEM detector with a single mask foil in reference [17]. Here a difference of a factor ~ 3.6 has been observed between the two orientations of the GEM foils. Based on this, the

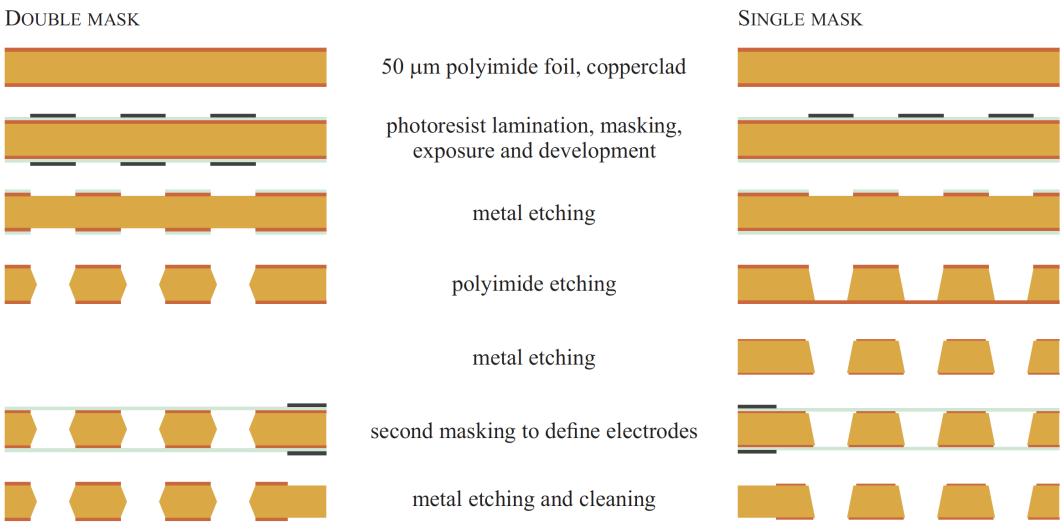

Figure 7: Schematic comparison of procedures for fabrication of a double-mask gem (left) and a single-mask gem (right) [16].

argument can be made that the measurements used in comparison with analytic calculations are performed with single mask GEM foils, while the simulations are done for double mask ones, effectively solving inconsistencies between theory and experiment. Nevertheless, this cannot be the only contributing factor to the discrepancy, as will be made clear with the SEG measurements in subsection 2.4. The goal of this subsection is to repeat this finding using the single GEM setup.

The orientation of the GEM foil in subsection 2.2 will be referred to as orientation 1 and the flipped foil as orientation 2. The same experimental procedure will be used to determine the effective gas gain for orientation 2. In figure 8, the effective gas gain of orientation 2 is plotted with its corresponding fit. The value of the fitted parameters of equation (3) are $a = 0.02188 \pm 0.00024$ V^{-1} and $b = -4.699 \pm 0.1070$ (no units). Considering the fact that the fit parameters of both orientations are within 2σ of one another, no significant gas gain difference can be concluded. The GEM is thus a double mask, or the asymmetry is such that the difference in gas gain and efficiency of the GEM cancel each other. In the next subsection, we will see that the former is true.

2.4 Cross section milling and SEG of the GEM

Knowing the precise geometry of the GEM holes in the foil used during the measurements can explain the observation made in the previous subsection. In addition, this geometry can be included in the modeling of the GEM in the simulations to have a more accurate one-to-one comparison with the measurement, although this falls beyond the scope of this paper.

With the use of focused ion beam (FIB) milling, cross-section SEG images of holes in the GEM foil can be made. This procedure was performed by Adrienn Baris, of the EN-MME-MM department at CERN, in the FIB room with me present. The resulting images are provided in figure 9 where the orientation of the foil corresponds to orientation 1. Since

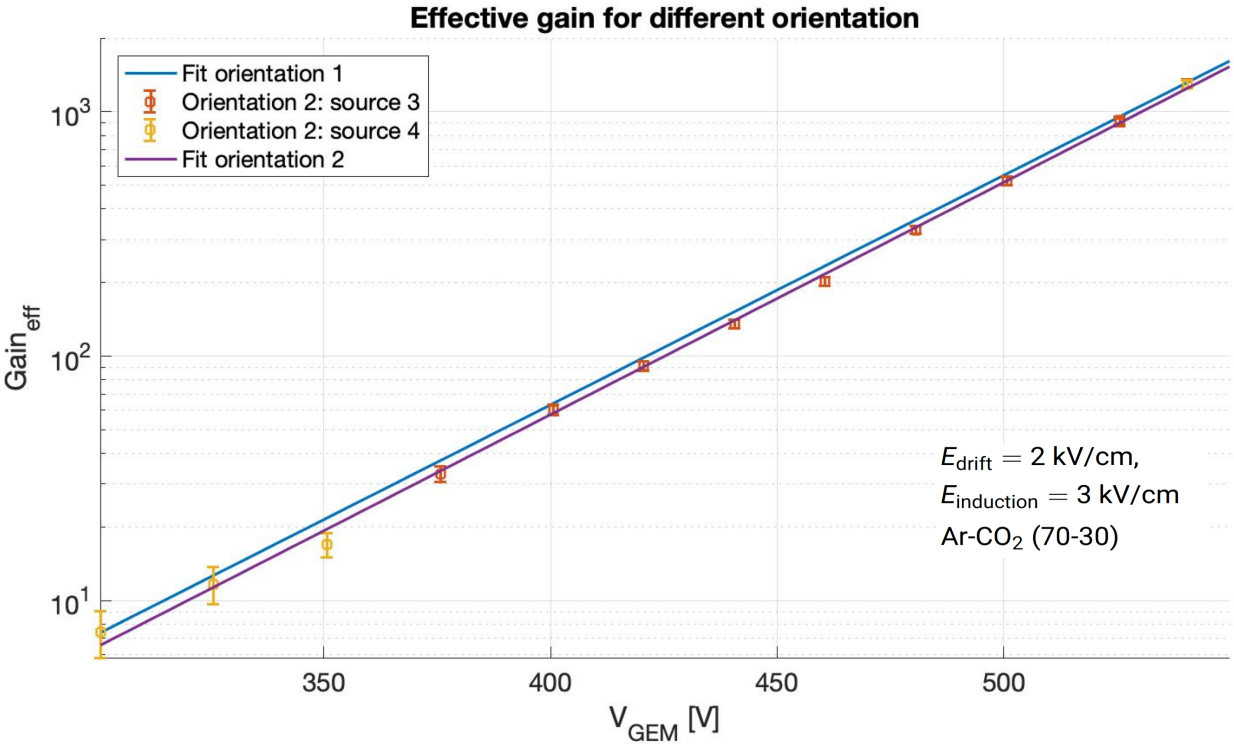

Figure 8: Measured effective gain for two different sources: 12.045 ± 0.602 kHz and 16.974 ± 0.8487 kHz for sources 3 and 4, respectively. The data points were fitted by the form (3) with Chi-square value $\chi^2 = 0.9987$. Comparison with the results presented in figure 5, no statistically significant difference in the gas gain can be observed.

the close resemblance with a double cone structure, the conclusion can be made that the foil was produced using the double mask technique. This most prominent asymmetry can be explained by a hole misalignment of 4.870 ± 0.005 μm, resulting in a shitted inner rim with 0.1321 ± 0.0110 rad. Nonetheless, this observation for this single hole can a priori not be extrapolated to the entire foil because of the local nature of these anomalies. Other forms of deformations come in the form of over etched copper, coves in the polyimide, and different diameters of the top and bottom opening of the hole. In our case, these are small compared with the misalignment. Due to the manufacturing method used and the nature of the asymmetry, the result of the previous section can be explained since flipping the foil yields a similar setup. These results show that the inconsistency between theory and experiment is present when both simulation and measurements are using double-mask foils.

2.5 Charge up effects

When applying the voltages and irradiating the detector, a transition period during which the effective gain changes has been observed. This is a well-documented behavior dubbed the charge up effect. During this period, significant alteration is the field configuration inside the holes will occur [7]. The reason is the accumulation of charges from the avalanches on the surface of the dielectric. As a result, the effective gain will be altered, and in general,

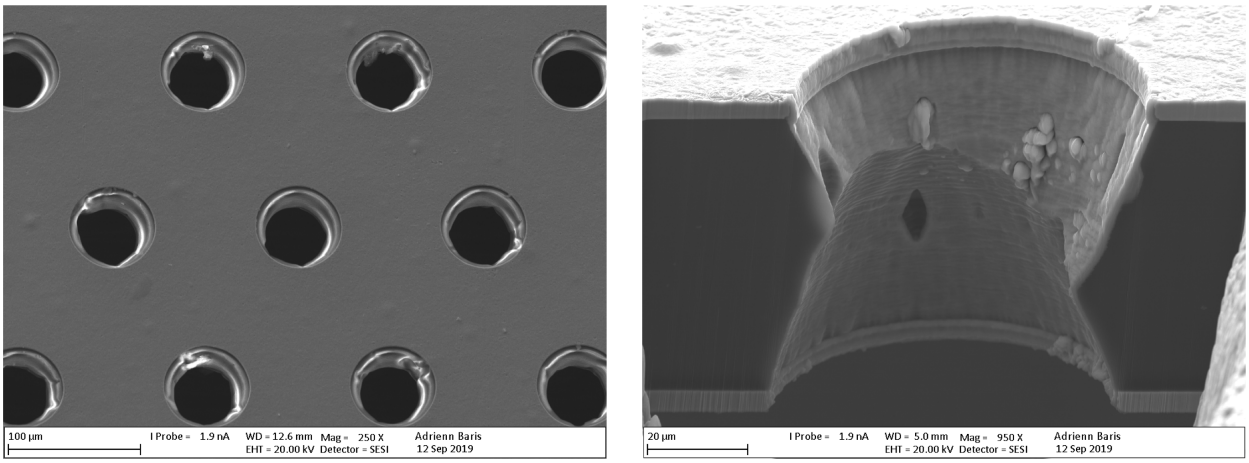

Figure 9: SEG images of the GEM foil which was used to perform the measurements. **Left:** Top view of the foil before FIB milling with the central hole being the one which has been studied. **Right:** Cross section view of a hole in the foil. The geometry is reminiscent of that of a double cone indicating a misaligned double mask manufacturing was performed.

an increase in the gas gain is observed until it saturates after approximately ~ 1.5 hours. This process is known to be rate-dependent, as shown in reference [22], where it is shown that the higher the rate of the source, the lower the measured gas gain. In addition, the polyimide used as the insulator has a higher conductivity, because it contains both intrinsic impurities and molecules picked up from the environment, e.g. polyamic acid, atmospheric ions and humidity. These are mobile and act as charge carriers, but contrary to electrons, they can neither leave nor be replenished through the electrodes [18, 19, 20, 21]. As a result, the current response to a potential difference is time-dependent. These effects cannot be overlooked since they are known to be able to contribute at least $10 - 15\%$ to the effective gain [7]. Due to the complex nature of these effects, the choice was made to measure the increase in effective gain due to these processes and scale down the measurements obtained in subsection 2.2. This allows for a better one-to-one comparison with the simulations performed in section 3, which do not include these charge up effects. In this subsection, an attempt is made at quantifying the increase in gain due to the charge up.

The measurements have been done in two parts: first the effect of the charge movement in the dielectric was established after which the effect of the charge accumulation was studied. For the former, the experimental procedure was the following. Immediately after switching on the voltages a low rate source, 51.20 ± 0.05 Hz, irradiates the detector long enough to take an MCA spectrum, after which the irradiation stops by placing a thick metal plate in between the detector and the source. This procedure takes 15 s and will be performed multiple times with at least 30 min from each other. The short exposure of the detector to the low rate source minimizes the charge buildup on the foil and thus, allows to study the effect of charge carriers in the polyimide on the gain. This effect is quantified by measuring the K_α peak position on the non-normalised scale of the MCA spectrum. After the saturation point was reached, the detector was continuously exposed for approximately 141 s to the low rate source, followed by continuously exposure to a high rate source of 5.31 ± 0.02 kHz until the plateau is reached. From the shift in the K_α peak position, the increase of the effective

gas gain due to charge up can be determined.

In figure 4, the results of both processes are shown. Here, the normalized gas gain is defined as the ratio between measured gas gain over time and the initially measured gas gain right after turning on the voltage. Despite observing an overall increase in the measured gas gain for both cases, the total saturation value of 1.4328 ± 0.0118 can deviate from the real scaling factor between an uncharged and charged GEM. Effects of changes in the environment such as pressure, temperature, and humidity were not measured and could possibly have occurred during the data taking. A ramping up period on the high voltages prevented immediate data taking, causing some ambiguity in the initially measured K_α peak position. In addition, unsuitability in the detector created sparks, which forced us to switch off and reapply the voltages across the electronics. These periods are marked in blue. However, since the aim of this project is to have a rough correspondence between theory and measurements, the obtained factor will be used to scale down the charged GEM data of figure 5, resulting in figure 11. This allows the discrepancy factor to reduce to 1.5681 ± 0.2889.

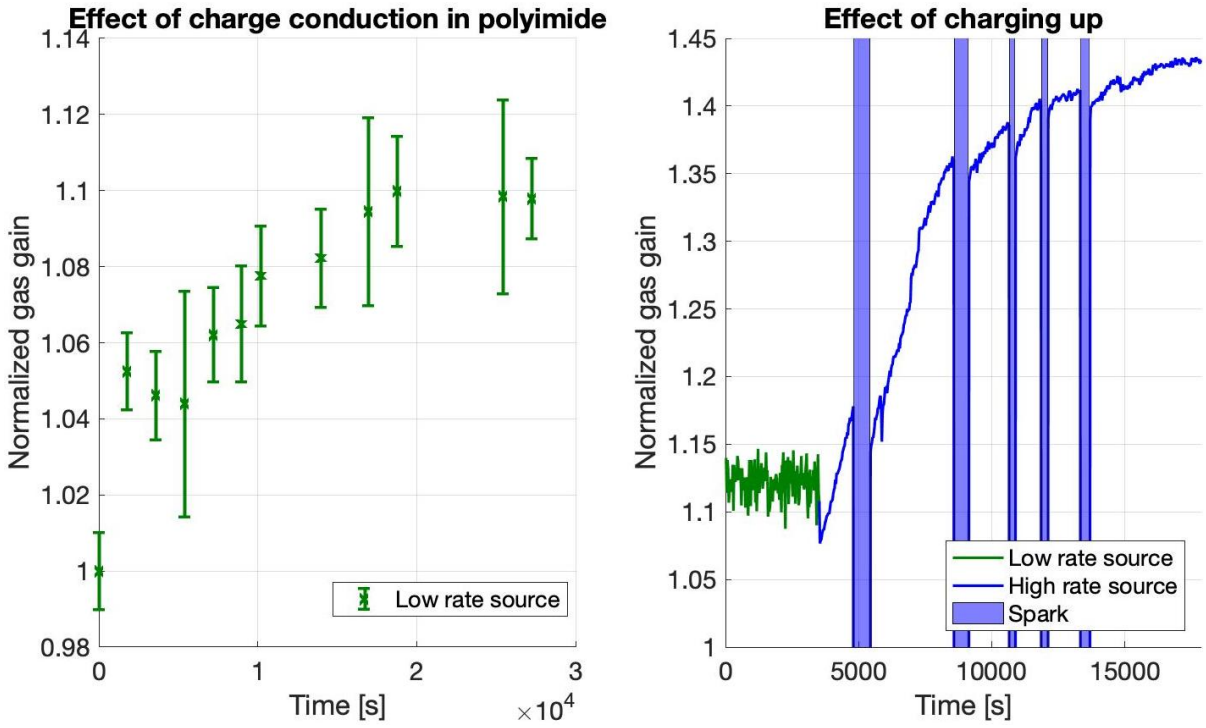

Figure 10: Effects on the measured gas gain over time when switching on voltages and irradiating the detector. Two source rates have been used: 51.20 ± 0.05 Hz (green) and 5.31 ± 0.02 kHz (blue). **Left:** Change in gain due to charge displacement in the polyimide of the GEM. **Right:** After the saturation of the charge displacement effect, the charge up effect due to charge buildup on the surface of the insulator was measured. In addition, the increase in the source rate shows an initial decrease in gain. This rate dependence is consistent with reference [22]. Periods of instability are indicated in blue, where a ramp down followed by a ramp-up of voltage was performed to reduce the sparking.

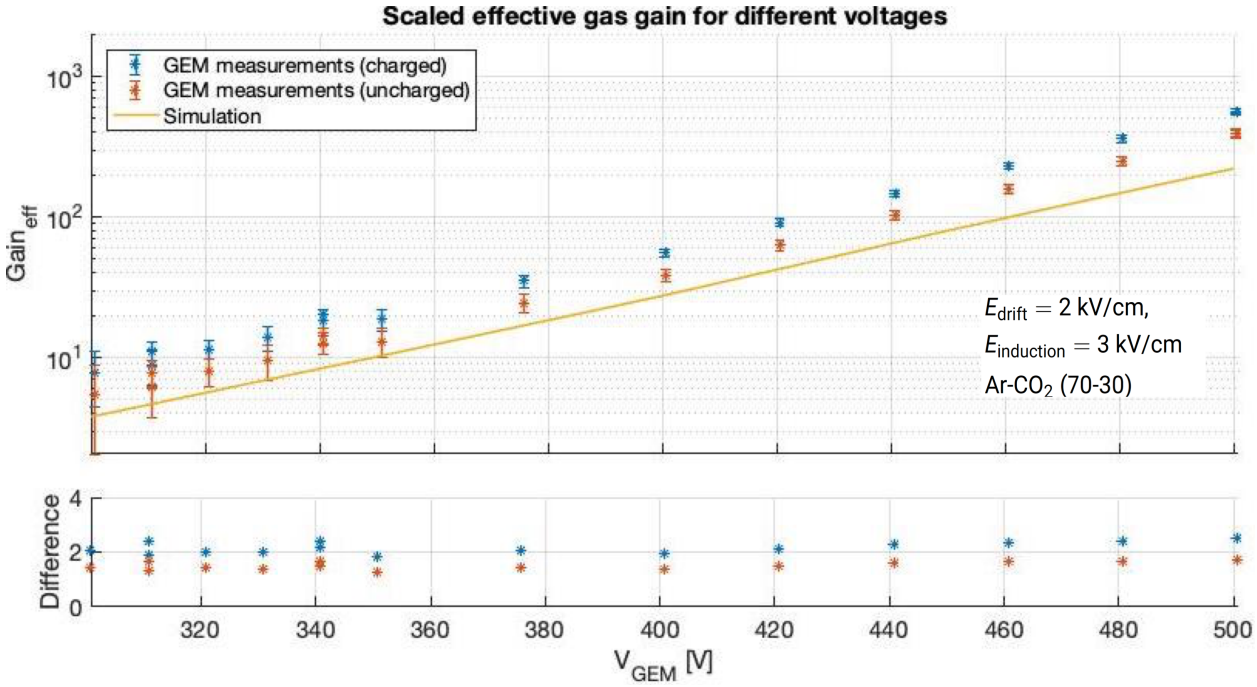

Figure 11: Scaled-down gas gain measurements of figure 5 to account for charge conduction in the dielectric and the charge up effect.

3 Simulations

3.1 Setup

The main software used for gas gain simulations in Micropatterned Gaseous Detectors is Garfield++ [8]. It interfaces with Magboltz to calculate the electron transport through the gas with penning transfer taken into account [23]. It can work in combination with models made in ANSYS® [24]. ANSYS is a commercially available finite element method (FEM) software that is used to design the geometry of the GEM and create maps of the electric field. Through scripting, a model of single GEM foil was constructed as a unit cell, which is a basic repetitive structure. Parameters for the ANSYS model are primarily those of the CERN standard single GEM described in table 1. However, in subsection 3.5 these will be altered in order to study the effects of variation in the geometry. The unit cell also includes drift and induction gaps where charge transport occurs, 2 mm, and 3 mm, respectively.

Effects of charge up and interaction between charges in the avalanches are not taken into account in these simulations. The former is overcome by using the rescaled measurements of subsection 2.5, while the latter can be neglected on the grounds that the discrepancy factor is also present for low rate and low gain setups. In these cases, only a few charges are present at any time in or around the GEM hole, giving no significant alterations in the field configuration of the system. The calculated absolute and effective gas gain ($\bar{G}$) are defined as the mean

$$\bar{G} = \frac{\sum_{i=1}^{n} G_i}{n}, \tag{4}$$

with n the number of simulated avalanches and G_i the absolute or effective gas gain of

avalanche i. The Γ distribution was not used in this project because it seemingly did not describe the obtained gas gain distributions [25].

In a gas mixture where an ionising radiation is incident, the input energy can be utilized in both ionisation and excitation depending on the interaction cross sections. The energy from excitation is primarily lost by a radiative or non-radiative transfer. However, if the excited state of one gas atom is higher than the ionisation potential of another gas present in the mixture, an excited state in the former gas atom, with some probability r_p, can give rise to an ionization in the latter. This process is called as Penning transfer. In the context of GEM detectors the Penning effect enhances the charge multiplication from the usual amount. This results in an increased gas gain. The ionization energy of 13,77 eV for CO_2 lies between the second and third excited states of Ar, 13 eV and 13,85 eV respectively. For an Ar-CO_2 is 70-30% a mixture this leads to a Penning transfer of $r_p = 0.56 \pm 0.03$ and will be included into the simulations [26].

The parameters of the simulations are the following (unless mentioned otherwise): $n = 1000$, $E_{\text{drift}} = 2$ kV/cm, $E_{\text{ind}} = 3$ kV/cm, mix of Ar-CO_2 is 70-30%, $r_p = 0.56$ for normal temperature and pressure (NTP). The resulting effective gas gain is plotted in figure 2 alongside with the measurements of the previous section. Only minor deviations can be found when comparing the calculations between Garfield-9 [27] and the more recent Garfield++ at $r_p = 0$; as plotted in figure 12. These differences can be explained by an improvement in the cross sections of Ar and CO_2 between the two versions.

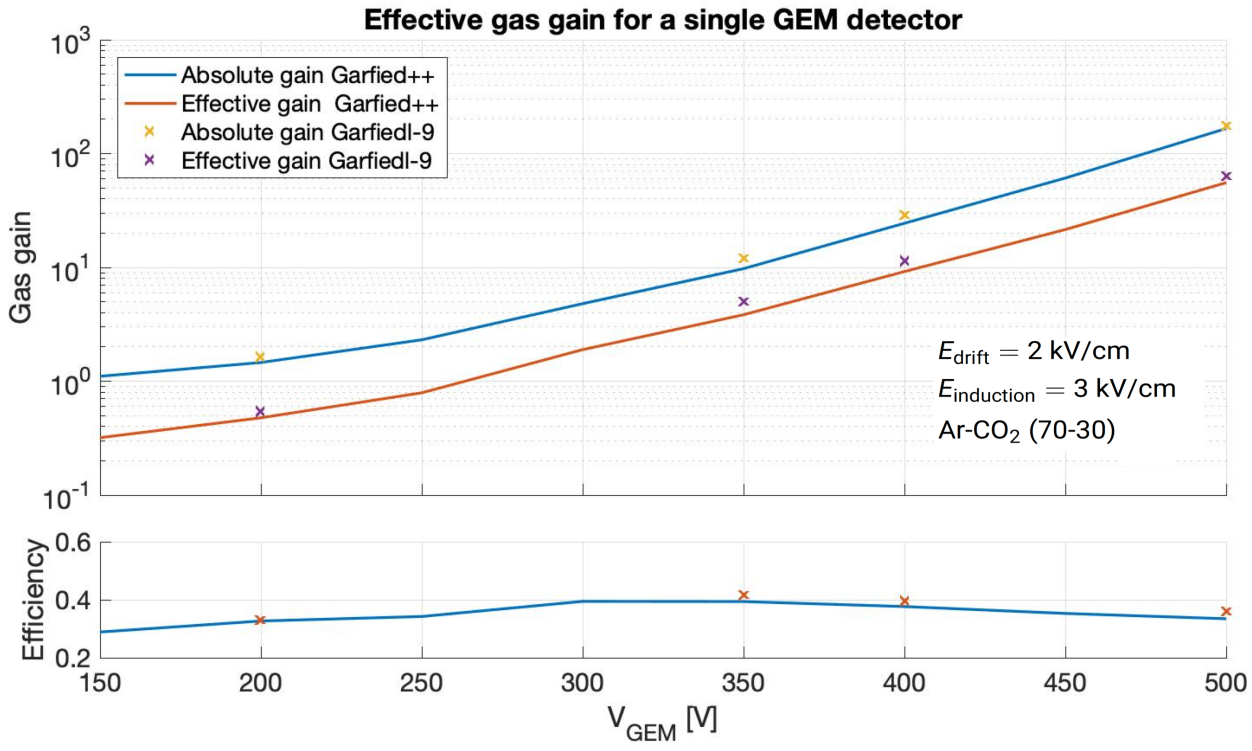

Figure 12: Comparison of absolute and effective gas gain simulations of between Garfied-9 and Garfield++ at $r_p = 0$.

3.2 Surface potential inside the GEM hole

The charge-up effect of a GEM, as explained in subsection 2.5, is not the only surface related effect that can alter the field configuration in and around a hole. In the presence of large amounts of charges, surface currents may occur, changing the electric fields. Using these currents, we were able to obtain a closed-form solution of the surface potential of the dielectric inside the hole.

The unit of choice is $\Omega/\square$ for the surface receptivity across any given square area of a polyimide, which is not dependent on absolute area, length, or thickness of the material. This way, one can model the surface of the polyimide as a series coupling of resistors with a current flowing through it. The reference frame is chosen to be centered in the middle of a single hole in the foil with the z-axis pointing upwards alongside the thickness of the foil. Modeling the geometry of the hole as a double cone, one can divide the surface into strips with area

$$A = \pi \sqrt{1 + \left(\frac{h}{R_{\text{top}}}\right)^2} (b^2 - r^2)\,, \tag{5}$$

where h is the height of the cone, R_{top} the radius of the outer hole, r the radius of a circle on the cone and b the radius of a different circle on the cone with $b > r$. The last two variables determine a strip placed on the surface of the cone of width $\Delta r = b - r$. Here only the upper half of the double cone structure will be used in the calculations, while the solution to the bottom halves can be retrieved by using the symmetry of the problem with respect to the xy-plane. The number of squares n_s with sides equal to the width of the strip is $A/\Delta r^2$. One can model the cone as a series coupling of resistors with resistance given by $R = R_S/n_s$. Using Ohm's law [28], the potential difference across the strip is given by

$$\Delta V = I\Delta R = \frac{I R_S \Delta r}{\pi \sqrt{1 + \left(\frac{h}{R_{\text{top}}}\right)^2} (\Delta r + 2r)}\,, \tag{6}$$

for an electrical current I. Taking the limit $\Delta r \to 0$ yields a differential equation with solution

$$V(r) = V_0 + \frac{I R_S}{\pi \sqrt{1 + \left(\frac{h}{R_{\text{top}}}\right)^2}} \ln\left(\frac{r}{R_{\text{top}}}\right), \tag{7}$$

where $V_0 = V$ is the potential on the upper copper layer of the GEM and $r \in [R_{\text{center}}, R_{\text{top}}]$. Figure 13 compares the analytical solution with the one obtained through ANSYS. Note that the qualitative behavior of the analytical solution is opposite to that of the finite element solution without the surface currents. This effect could impact the gas gain inside the hole of the GEM in addition to altering the drift of the electrons. However, this solution is only valid in the presence of a large amount of charges inside the hole, i.e. for high rate or large gain. Therefore, this avenue of exploration was sidelined in favor of the ones in the next subsections.

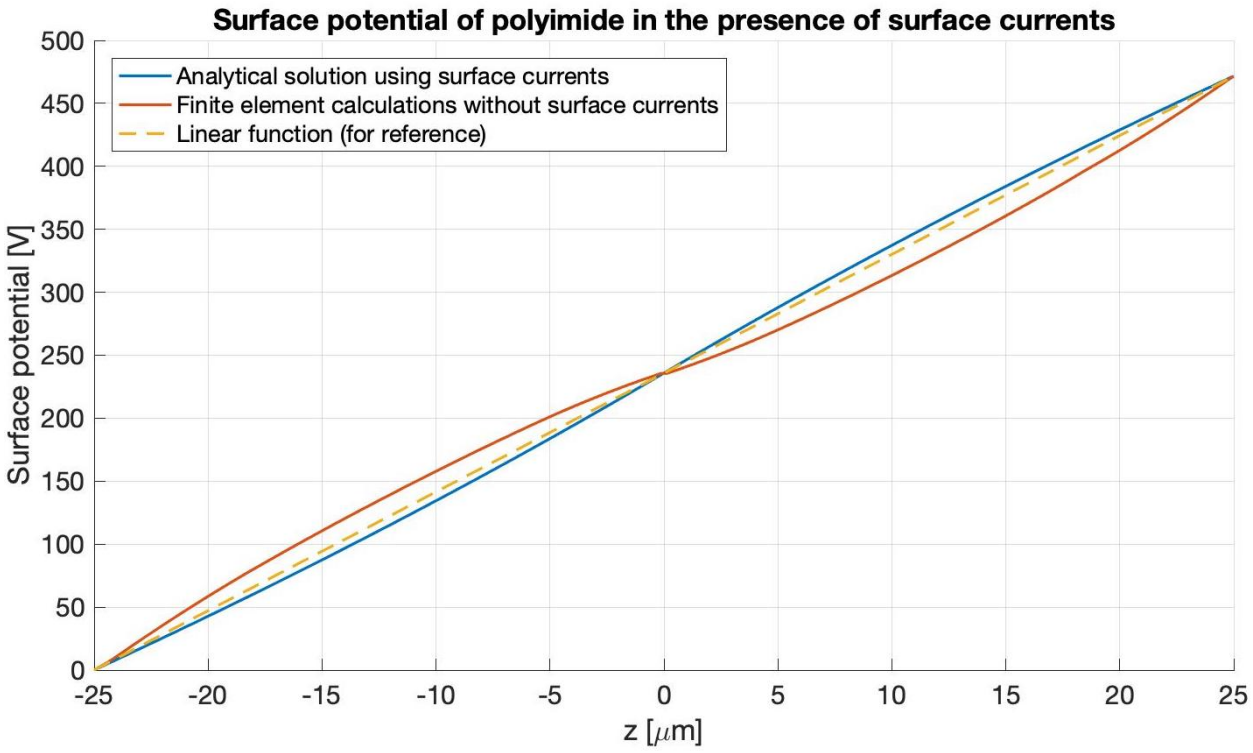

Figure 13: Surface potential of the dielectric inside a GEM hole using finite elements calculations (ANSYS) without surface currents and analytical calculations with surface currents. Here an R_S of $3.6 \cdot 10^{16}$ $\Omega/\square$ was used [29].

3.3 Electron transport algorithm

The Monte Carlo algorithm, which is used in Garfield++ for the electron transport, is based on the collision rate, which is a function of the electron energy of the particle. Because of the electric field, the electron energy and the collision rate do, however, vary during the free flight step. This can be taken into account using the so-called null-collision technique [30]. Using this algorithm, a free time Δt can be obtained based on the energy of the particle after Δt. To determine the energy, the position, and velocity after Δt a constant field approximation is used. Here the electric field $\vec{E}$ is taken to be constant during the free path of the particle, which takes on the value of the field at the initial point of the electron. This approximation is valid for systems where the field variations are small during the mean free path of the electron. However, this is not a trivial statement to make for the GEM. For example, in the neighborhood of the copper edges, significant variations of the field strength can be observed. As a result, the calculated trajectories of the electrons could significantly deviate from reality. Based on this argument, we have implemented a more accurate electron transport algorithm in Garfield++ and look how it differs from the original model.

The algorithm used for this is the Runge-Kutta-Nyström method to solve the Lorenz equation based on the ANSYS finite element field map of the GEM detector [31]. A difference of $3.15 \pm 0.55\%$ can be observed after the implementation of the Runge-Kutta-Nyström method, suggesting that the constant field approximation only results in minor deviations. However, in the case of low pressures, the mean free path of the electron can become bigger

than the thickness of the GEM foil. This can lead to simulation results which do not only give significant deviations from the correct trajectory, but in addition, causes the electrons to seemingly go through the GEM foils' solid material. For this reason, work is being done with Heinrich Schindler of the EP-LBO-DO department at CERN to incorporate the Runge-Kutta-Nyström method into the main branch of Garfield++, enabling users to study gas gain in low-pressure systems.

3.4 Secondary electron emissions dependency

As the electrons collide with the dielectric surface, they either stick to the surface, charging it negatively, or release secondary electrons from the surface leaving behind positive charge. This process is known as secondary electron emission. This possibility of secondary electron emission (SEE) of the polyimide is not incorporated into the simulations. In this subsection a qualitative estimate will be made of the contribution of this effect to the gas gain.

In figure 14 the SEE coefficient δ is given for Kapton® [32]. Note that the energy regions where δ <1 are the cases where the primary electrons stick to the surface without ejecting any new charges. In addition, there is a maximum number of secondary electrons released from the surface (δ_m), which occurs when the primary electron has an energy of ε_m. The energy distribution of electrons colliding with the polyimide, is shown in figure 14. Considering that the minimum energy necessary to eject charges from the surface is $\varepsilon_I = 30$ eV, the amount of incoming electrons which can release charge is small, based on the overflow value of 7 in figure 14 [32]. Furthermore, electrons that do get released by the SEE effect must have enough initial energy to go against the field lines in some regions in order to avoid sticking to the surface. Thus, the ejected charges need to have a certain escape velocity. This suggests that the SEE for polyimide has a minor contribution and can be neglected in the simulations. This conclusion can a priori not be generalized to all secondary emissions, e.g.

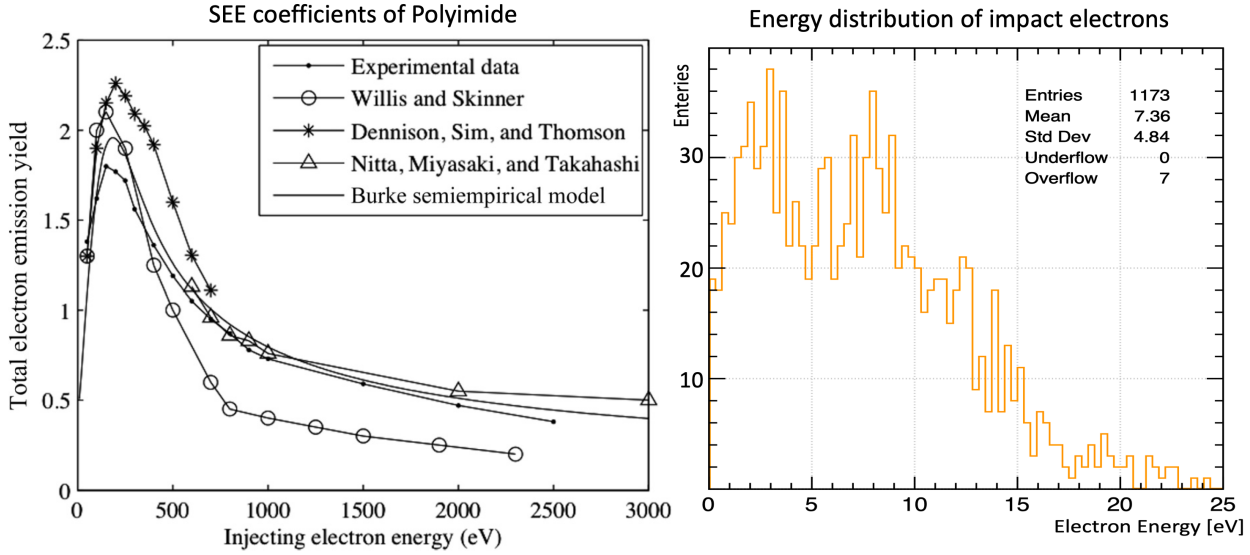

Figure 14: **Left:** Secondary electron emission coefficient of the Kapton as a function of the energy of the colliding electron [32]. **Right:** Energy distribution of colliding electrons as obtained from simulations.

the photoelectric effect or de-excitation photons on copper which only has a work function of 5.10 eV [33]. However, the argument of having a certain escape velocity is still true. Additional research has to be done to get a full picture of the significance of the absence of these effects in the simulations.

3.5 Hole geometry dependency

This final subsection will be a continuation of the remarks made in subsection 2.3 concerning the geometry of the hole. As mentioned deformations with respect to the standard GEM hole geometry can occur coming form the manufacturing processes used. More common deformations include: variations in the hole sizes, variations in the thickness of the copper layer, over etched copper sheets and off-centering of the inner ring of the double cone. Here, the effects on the absolute and effective gas gain due to asymmetries in the GEM will be simulated.

Figure 15 shows the effective and absolute gas gains for different types of asymmetries. Shifting up the inner circle of the double cone upwards increases the inefficiency by 22%, while leaving the effective gas gain almost unchanged. A decrease in the bottom outer hole size form 70 μm to 30 μm decreases the effective gas gain by 56% while an increase to 100 μm gives a decrease of 62%. The mirror to these geometries gives a maximum difference of 71% in the effective gas gain. Since the avalanches are primarily created in the volume around the bottom outer hole, increasing the electrical field strength here should increase the gas gain. Despite this, when introducing 10 μm of overhanging copper to the bottom metal layer: an increase of 3% in the absolute gas gain is observed. Finally, a 4% increase in effective gas gain by reducing the metal thickness from 5 μm to 1 μm of the bottom copper layer while for the top layer a decrease of 7% can be observed. These results not only explain possible differences in gas gain measurements between different GEM foils, but also allow for the engineering of more optimal hole geometries.

4 Conclusion

My CERN summer student project was centered around the discrepancy between experimental en theoretical results of the effective gas gain of single GEM detectors. Figure 2 compares measurements of different batches of CERN standard GEM foils (table 1) with simulations of uncharged foils of the same type. A difference factor of 2.2468 ± 0.2640 was observed, which cannot be explained by the charge up effect as it only lowers the difference factor to 1.5681 ± 0.2889 (figure 11). The single GEM detector simulations were performed using Garfield++ and ANSYS with the parameters of the model matching those of the experimental setup used. A better understanding of the physics of these types of micro-pattern gaseous detectors could prove useful for the improvement of such detectors. Despite not being able to resolve this discrepancy during this project, some other results were obtained in the process.

The experimental setup used is given in figure 3, here electrical field strengths $E_{\text{drift}} = 2$ kV/cm and $E_{\text{ind}} = 3$ kV/cm were used in order to compare our results with reference [2]. Figure 6 indicates that the measured gas gain has a strong dependence on E_{ind} and a weak

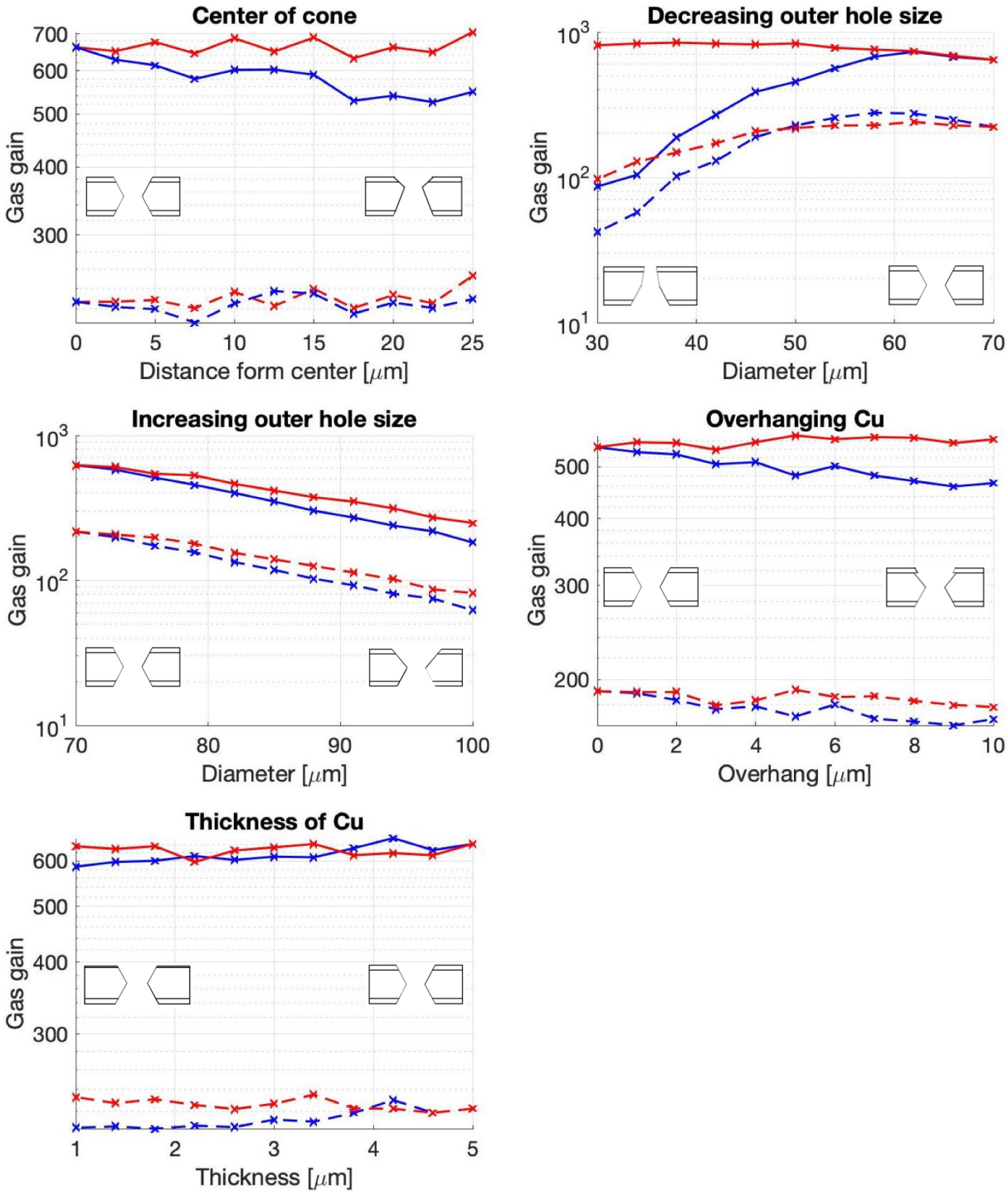

Figure 15: Simulated effects of the hole geometry on the gas gain for $V_{\mathrm{GEM}} = 500$ V. Reference point is summed up in table 1. Respectively the blue and red curves represent the variation in parameters on the upper and bottom half of the GEM while keeping the other half unchanged. The full lines indicate the absolute gas gain while the dashed lines indicate the effective gas gain.

dependence on E_{drift} as long that it is in the plateau region. This suggests that one-to-one comparisons of measurements of different references, such as in figure 2, ideally need to have the same E_{ind} value. Our measurements were performed using a misaligned double-mask GEM foil, as shown in the scanning electron microscope images (SEG) in figure 9. The characteristic of the geometry of the hole of the GEM allowed for a statistically insignificant difference in the effective gas gain when flipping the orientation of the foil, as can be seen in figure 8. This is in agreement with reference [17] where similar measurements were performed with a triple GEM detector comprised of double-mask foils. However, the same reference shows a factor of ~ 3.6 of difference in the effective gas gain between the two orientations of single-mask foils due to their asymmetry in the hole structure. Five types of asymmetries and their effect on the gas gain have been studied using simulations. These results can be found in figure 15 with the most prominent effects coming from the outer hole sizes of the GEM. Differences between measurements performed by similar setups can be explained using these results.

On the simulation side of the project, we expanded the existing electron transport algorithm of Garfield++ with the Runge-Kutta-Nyström method. Originally the transport was calculated by taking the electric field to be constant during the free path of the particle, which is a valid approximation for small changes in the electrical fields with respect to the mean free path of the electron. However, it is a priori unclear if this approximation holds for the GEM where regions of fast changing electrical field values are present, e.g. at the edges of the copper. Solving the Lorentz force equation using Runge-Kutta-Nyström method gives no significant improvement of gas gain simulations at atmospheric pressure. In spite of this result, the algorithm can prove useful to study low-pressure gaseous detectors since the mean free path becoming larger than the thickness of the GEM foil, leading to electrons going through the metal and dielectric layers. In addition, we looked at the contribution of secondary electron emissions to the gas gain. Based on figure 14, this effect can be neglected in simulations. A final result is an analytical calculation of the surface potential of the polyimide inside a hole in the presence of a surface current. The resulting equation (7) shows an opposite qualitative behavior as opposed to the ANSYS results without surface currents (figure 13). This process will only occur at high gas gains or with high rate sources, thus not explaining the discrepancy between theory and experiment over the full spectrum of the voltage across the GEM.

With the results obtained during the project, some future steps can be suggested. An ANSYS model could be constructed using the exact SEG measurements of the GEM foil used. This allows for a better one-to-one comparison between theory and our experimental results, leading to a more precise estimate of the discrepancy factor. One could expand the types of asymmetries that were studied and start to mix them to have a complete overview of the effects of the geometries of manufactured GEM foils. A study of low-pressure gaseous detectors can be made using the altered electron transport algorithm and compare it to measurements. Finally, equation (7) could be set as a boundary condition on the ANSYS model in order to study the difference in the trajectories of the charges in the presence of surface currents.

5 Acknowledgements

This work would not have been possible without the help and kindness of a few people who I would like to thank.

The first person that I would like to acknowledge is Rob Veenhof. Over the almost three months we worked together you absolutely exceeded your role as my CERN supervisor. Before starting the summer project, I had no prior knowledge of the working principals of MPGDs, which was out of my usual field of study. Your invaluable guidance and mentoring helped me explore this exciting field of research and let me obtain new and important skills as a researcher. Our regular discussions were refreshing and genuinely something I looked forward to every time. The balance you wielded between closely following my progress and giving me the freedom to work freely during the project was a pleasant one. The endless stream of stories you provided during, but not excluded to, the numerous coffee and cake breaks always sheered me up. I must admit to retelling a few of them back in Belgium. I hope that we will continue to collaborate in the future.

The second person I want to thank is Eraldo Oliveri. I was quite hesitant when hearing that I needed to perform measurements inside a lab during the project, since this was outside my usual comfort zone. Thanks to your guidance and infectious enthusiasm, I discovered that I actually love doing it. This not only opens up new possibilities for me but also enabled me to produce lab work that I am proud of. Not to forget, the high standard of coffee you provided to the group kept me happy and productive the whole day through. It was my pleasure of having you as my CERN supervisor, and I hope we can again work together in the future.

In addition, I want to express my gratitude to Heinrich Schindler for his patience with my countless questions about Garfield++, C++, etc. I cannot stress enough how vital your help was to me during this project. Despite your busy schedule, you were always quick to respond and willing to make some time for me. I enjoyed our meetups in R1 to drink coffee and discuss the programming part of the project. I have learned a great deal about C++ from you, and thanks to you, I am not afraid anymore to open the terminal window on my computer. It was an honor working with you, and I hope our paths cross again soon.

In general, I want to thank the entire RD51 collaboration for giving me the opportunity to work on this project. I greatly benefited from many interesting discussions of this group. You made my summer one remember.

Finally, I want to thank the CERN summer student program for making this project possible.

References

[1] F. Sauli, "GEM: A new concept for electron amplification in gas detectors," Nucl. Instrum. Meth. A **386** (1997) 531.

[2] G. Croci, "Development and Characterization of Micro-Pattern Gaseous Detectors for HEP applications and beyond," PhD thesis, University of Siena (2010).

[3] F. Sauli, "Gaseous Radiation Detectors : Fundamentals and Applications," Camb. Monogr. Part. Phys. Nucl. Phys. Cosmol. **36** (2014) pp.1.

[4] CMS Collaboration, https://cms.cern/detector/detecting-muons/gas-electron-multiplier, accessed at 10 October 2019.

[5] J. E. Brücken *et al.* [ALICE TPC upgrade Collaboration], "The GEM QA Protocol of the ALICE TPC Upgrade Project," PoS MPGD **2017** (2019) 073 [arXiv:1811.07043 [physics.ins-det]].

[6] A. Cardini [LHCb Muon Upgrade Group], "The LHCb Muon Upgrade," JINST **9** (2014) C02014.

[7] P. M. M. Correia *et al.* [CERN RD-51 Collaboration], "A dynamic method for charging-up calculations: the case of GEM," JINST **9** (2014) P07025 [arXiv:1401.4009 [physics.ins-det]].

[8] H. Schindler, "Garfield++ simulation of tracking detectors," http://garfieldpp.web.cern.ch/garfieldpp/.

[9] M. Nemallapudi, "Gain of a single gas electron multipier, " Master thesis, SASTRA University (2008).

[10] CAEN S.p.A, https://www.caen.it, accessed at 20 September 2019.

[11] ORTEC/AMETEK Inc., https://www.ortec-online.com, accessed at 20 September 2019.

[12] AMETEK Inc., https://www.amptek.com, accessed at 20 September 2019.

[13] Tektronix Inc., https://www.tek.com, accessed at 20 September 2019.

[14] H. Schindler, "Microscopic Simulation of Particle Detectors, " PhD thesis, Technischen Universitt Wien (2012).

[15] Private communication with the CMS GEM team (2019).

[16] S. Pinto, "Progress on large area GEMs," Journal of Instrumentation, Volume 12, Issue 12, pp. 009 (2009).

[17] J. Merlin, "Study of long-term sustained operation of gaseous detectors for the high rate environment in CMS," University of Strasbourg (2016).

[18] R. Barker Jr., "Mobility and Conductivity of Ions in and into Polymeric Solids," Pure Appl. Chem. **46** (1976) 157170.

[19] H. Oji *et al.*, "Thermal Imidization Reaction of PMDA-ODA Polyimide Studied by NEXAFS Spectroscopy," Memoirs of the Synchrotron Radiation Center, Ritsumeikan University, Kyoto, Japan 8 (2006) 187188.

[20] E. Sacher, "Dielectric Properties of Polyimide Film. II. DC Properties," IEEE Transactions on Electrical Insulation **EI-14** (1979) 8593.

[21] G.M. Sessler *et al.*, Electrical conduction in polyimide films, Journal of Applied Physics **60** (1986) 318326.

[22] L. Arazi *et al.*, " Laboratory studies of THGEM-based WELL detector structures with resistive anode," JINST 9 P04011 (2014).

[23] S. Biagi, "Magboltz- transport of electrons in gas mixtures, " http://consult.cern.ch/writeups/magboltz/. 31, 35, 38.

[24] ANSYS Inc., ANSYS version 16.1 Electromagnetics (2010).

[25] F. Eggenberger *et al.*, "Über die Statistik verketteter Vorgnge," Zeitschrift fr Angewandte Mathematik und Mechanik **3** (1923) 279289.

[26] Ö. Şahin *et al.*, "Penning transfer in argon-based gas mixtures," JINST **5** (2010) no.05, P05002.

[27] R. Veenhof, "Garfield simulation of gaseous detectors," http://garfield.web.cern.ch/garfield/.

[28] D. Griffiths, "Introduction to electrodynamics, " Pearson (2013).

[29] DuPont Films, "Corona Resistant Kapton CR Takes Electrical Insulation Design and Reliability to New Levels," https://www.dupont.com, accessed at 24 September 2019.

[30] H. Skkullerud, "The stochastic computer simulation of ion motion in a gas subjected to a constant electric field, " J. Phys. D: Appl. Phys. **1** 1567 (1968).

[31] E. Lund, "Track parameter propagation through the application of a new adaptive Runge-Kutta-Nyström method in the ATLAS experiment, "Journal of Instrumentation, Volume 4 (2009).

[32] Y. Chen *et al.*, "Total electron emission yield measurement of insulator by a scanning small detector," Applied Physics Letters **99**, 152101 (2011).

[33] D. Lide, "Handbook of Chemistry and Physics," CRC Press (2008).